INSTITUTE OF PHYSICS PUBLISHING JOURNAL OF PHYSICS: CONDENSED MATTER

J. Phys.: Condens. Matter **13** (2001) 6977–6991 PII: S0953-8984(01)24778-X

Structural analysis of InGaN epilayers

K P O'Donnell[1], **J F W Mosselmans**[2], **R W Martin**[1], **S Pereira**[1,3] **and M E White**[1]

[1] Department of Physics and Applied Physics, University of Strathclyde, Glasgow G4 0NG, UK
[2] Synchrotron Radiation Department, CLRC Daresbury Laboratories, Warrington WA4 4AD, UK
[3] Departamento de Física, Universidade de Aveiro, 3810-193 Aveiro, Portugal

Received 11 May 2001
Published 26 July 2001
Online at stacks.iop.org/JPhysCM/13/6977

Abstract

The structural properties of InGaN have attracted interest on account of the recent widespread use of the material in visible light-emitting devices. A key topic has been the indirect determination of the composition by x-ray diffraction (XRD). We examine critically the several levels of approximation involved in this procedure. It is shown by extended x-ray absorption fine structure (EXAFS) measurements that the local structure of InGaN is *independent* of the composition, in the range of InN fraction, from about 15 to 40%, that corresponds to blue to infrared light emission from this material. EXAFS-determined ratios of the numbers of indium and gallium atoms in the first metal co-ordination shell, M1, show very good agreement with the composition measured by established techniques, both structural and chemical, on similar samples. On the other hand, the atomic separations deviate markedly from values calculated using Vegard's law. In particular, the average radial separations, In–N1 = 2.11(2) Å and In–M1 = 3.28(3) Å, do not vary significantly with In/Ga ratio in the examined composition range. We conclude with some brief comments on the uncertain but challenging topic of InGaN nanostructure.

1. Introduction

The high efficiency of luminescence from InGaN/GaN heterostructures has underpinned recent developments in blue–green optoelectronics [1]. A qualitative understanding of the nature of this luminescence is slowly emerging. Localization of excitation, whether by alloy composition fluctuations [2] or in self-formed quantum dots [3], appears to tilt the balance in favour of radiative recombination, despite the observation by electron microscopy of huge densities of extended defects in 'device-grade' material [4]. The peak energy of photoluminescence (PL) emission from thick InGaN epilayers depends upon the mean indium nitride content, assessed by a wide range of independent techniques, in a simple, linear way [5]. Furthermore, the PL peak is down-shifted from the corresponding absorption or excitation band edge by an energy,

Stokes' shift, that also depends linearly on the indium nitride fraction [6]. What remains unclear about InGaN, after a great deal of work, is the relationship between its composition and nanostructure, and whether an understanding of this relationship can lead to an explanation of the *origin* of InGaN luminescence.

It is important to note that accurate assessment of the structure and composition of ultrathin layers of semiconductor material ($\leqslant$3 nm thick) is an unsolved technical problem. However, such layers form the active regions of working nitride devices. Composition values of thick layers determined by chemical techniques, such as Rutherford backscattering spectrometry (RBS), sputtered ion mass spectroscopy (SIMS) and electron probe microanalysis (EPMA), are truly insensitive to the state of strain in a sample: the signal strength for each atomic species, such as In, depends directly on the number of atoms of that species present in the sample. On the other hand, XRD measures structural parameters directly, but it is an indirect technique when used to measure composition. Routine determination of alloy composition from XRD data should take the sample's state of strain properly into account. We show here that EXAFS is sensitive both to the structure and the composition of InGaN epilayers.

We have argued previously that, contrary to accepted wisdom, current theoretical models fail to give a satisfactory account of the dependence of the optical energies on the composition of InGaN [7]. Furthermore, there has been a great deal of discussion in the literature about the influence of strain, phase decomposition, ordering, disordering etc on the optical energies of InGaN, and even some confusion about how to measure these energies, and what they represent. The following review attempts to clarify some of these points of uncertainty. The layout of the review will be as follows. In section 2, we describe the technique of XRD applied to the determination of InGaN alloy composition. In section 3 we present recent EXAFS work on the local structure of InGaN epilayers. In section 4, we discuss models of InGaN nanostructure, with particular reference to the optical properties.

2. Use of XRD in the determination of alloy composition

XRD measures the average values of the lattice constants of possibly strained layers. In favourable circumstances, it can also measure their thickness. Figure 1(a) shows a θ–2θ scan of GaN and InGaN (00.2) diffraction peaks from a representative InGaN/GaN bilayer. The lattice constants in the growth direction, c(GaN) and c(InGaN), for any allowed (00.l) reflection, are given directly by Bragg's law:

$$c = l\lambda/(2\sin\theta_B) \tag{1}$$

using radiation of wavelength λ (in our case Cu Kα_1) and with the relevant Bragg angle, θ_B, estimated from the peak of the XRD distribution. For the example shown here, the respective lattice constants obtained by use of equation (1) are c(GaN) = 5.1838 Å and c(InGaN) = 5.2516 Å. In a similar way, a scan through the asymmetric (10.5) reflection, shown in figure 1(b), provides estimates of the lattice parameters a(GaN) = 3.1908 Å and a(InGaN) = 3.207 Å.

In the case of biaxially strained wurtzite structures, such as InGaN/GaN, distortion of the hexagonal unit cell occurs. In order to separate the influence of strain and composition, both parameters of the wurtzite lattice, c(InGaN) and a(InGaN), should be measured and compared to their relaxed values.

By definition, the ratio of the vertical to the lateral strain is

$$\xi(x) = -\frac{c(\mathrm{InGaN}) - c_0(x)}{c_0(x)}\,\frac{a_0(x)}{a(\mathrm{InGaN}) - a_0(x)} \tag{2}$$

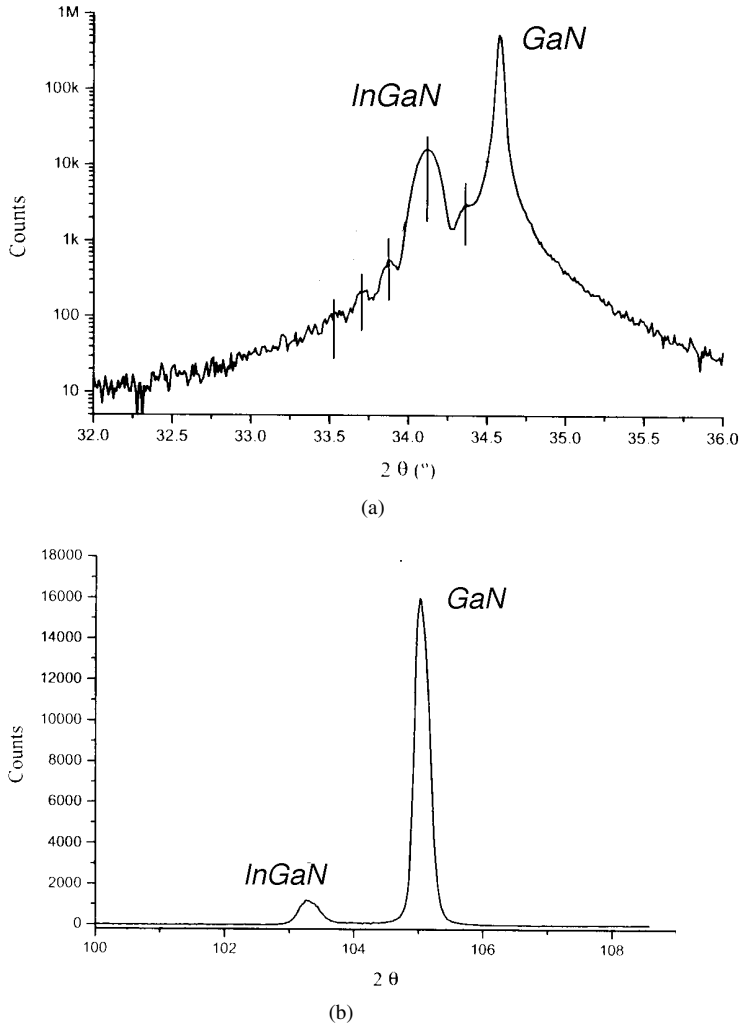

Figure 1. XRD analysis of an InGaN/GaN bilayer, showing the InGaN and GaN peaks in (a) symmetric (00.2) and (b) asymmetric (10.5) scans.

where $c_0(x)$ and $a_0(x)$ are the relaxed lattice constants. In order to determine the composition from the measured lattice constants, we can evaluate both sides of equation (2) separately and seek the value of x at which they coincide. This procedure is illustrated in figure 2(b). According to Vegard's law, the lattice constants for a given value of x can be calculated by a linear interpolation between those of the binaries, GaN and InN. ξ is related to Poisson's ratio and can also be interpolated from the measured or calculated binary values.

Symmetric XRD reflections measure only the out-of-plane lattice constant, c(InGaN), but are stronger and easier to obtain experimentally than asymmetric reflections. In the absence of further information, it is customary to consider one or other of the following two extreme situations.

(i) Layers may be fully relaxed: $c(\text{InGaN}) = c_0$. This assumption is likely to be justified when layers are relatively thick. According to Vegard's law, the *relaxed* lattice constant

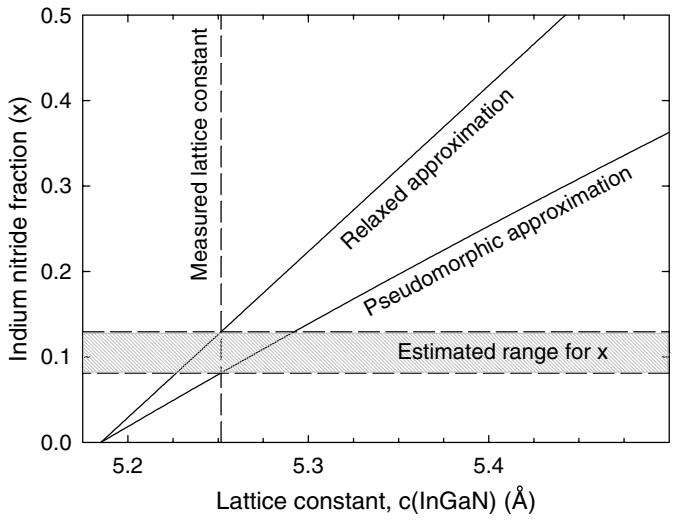

(a)

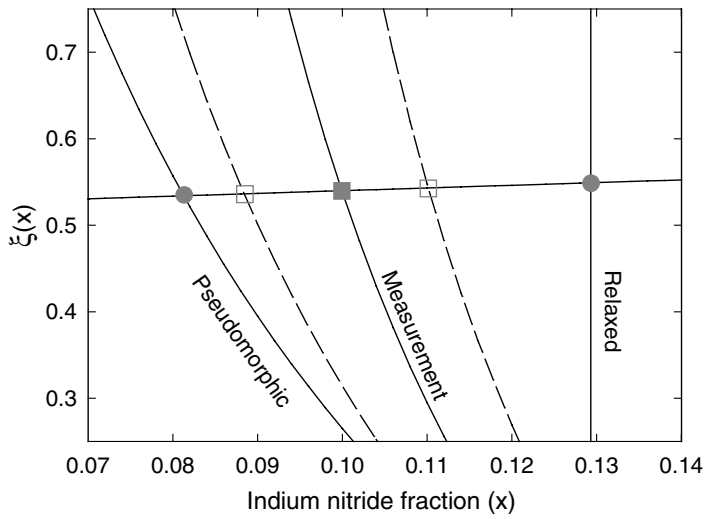

(b)

Figure 2. Estimation of the indium nitride content, x, from a measurement of the lattice constants. (a) Illustration of the range for x resulting from the approximations of a fully relaxed and pseudomorphic InGaN layer. (b) Graphical solution of equation (2) using the measured lattice constants from figure 1, along with the relaxed and pseudomorphic approximations. The broken lines either side of the 'measured' curve represent estimated uncertainties of $\pm 0.01^\circ$ and $\pm 0.04^\circ$ in θ for the symmetric and asymmetric scans, respectively.

$c_0(x)$ of the binary mixture of compounds, $In_xGa_{1-x}N = xInN : (1-x)GaN$, scales linearly with x:

$$c_0(x) = c(\text{GaN}) + x(c(\text{InN}) - c(\text{GaN})) = (1-x)c(\text{GaN}) + c(\text{InN}). \quad (3)$$

Hence x can be determined immediately from c(InGaN) (assumed to be the same as c_0) if 'relaxed' values of c(GaN) and c(InN) are known. Benchmark values of the relaxed

lattice constants are available from measurements on 'bulk' crystals of binary materials. A locally determined value of c(GaN) may be preferred as a first order correction in the case of InGaN epilyers grown on GaN.

(ii) Layers may be pseudomorphic: a(InGaN) $= a$(GaN). In pseudomorphic growth, a thin epilayer accommodates itself to a thick substrate. This is often the case for InGaN layers of thickness less than about 75 nm, grown on GaN pseudosubstrates. With the assumption that the in-plane lattice constants of epilayer and substrate are equal, x can again be estimated, knowing only c(InGaN), by solving equation (2).

The partial relaxation expected in real samples, or in ideal samples of intermediate thickness, is an important issue. If the assumption is made that relaxation is always complete, the indium nitride fraction will be consistently overestimated. Indium nitride fractions tend to be underestimated if layers are assumed to be pseudomorphic. Figure 2(a) illustrates the point for our representative example, with a measured c(InGaN) $= 5.2516$ Å. If a(InGaN) is not measured, we can infer from the XRD measurement only the fact that the indium nitride fraction falls between 8.1% and 12.9%. The range of uncertainty in estimating x in this way obviously increases with increasing InN content. On the other hand, if a(InGaN) is also known, we can readily determine x, as shown in figure 2(b). The intersection point of the curves,

$$y_1 = \xi(x) \qquad y_2 = -\frac{c(\text{InGaN}) - c_0(x)}{c_0(x)} \frac{a_0(x)}{a(\text{InGaN}) - a_0(x)}$$

gives the required solution. An uncertainty remains in choosing the actual value of the elastic constants used to calculate $\xi(x)$ experimental values being scarce and scattered. In a narrow range of x, this ratio is expected to be fairly constant, as shown here using the widely accepted theoretical estimates of ξ(GaN) $= 0.509$ and ξ(InN) $= 0.821$ [8]. Further purely experimental uncertainties in measuring c(InGaN) and a(InGaN) lead to a surprisingly high final error in x. While our best value of $x = 10.0\%$ is obtained by adopting a(InGaN) $= 3.207$ Å, a value of a(InGaN) $= 3.210$ Å, higher by only one part in a thousand, would raise the estimate to 11%. Note that RBS measurements from the same sample gives $x = 0.10 \pm 0.01$, coinciding almost exactly with our XRD estimate. Closely spaced satellite peaks in XRD, indicated by vertical bars in figure 1(a), allow a direct estimate of layer thickness, in this case 45 nm. There is good agreement between this value and that obtained, less directly, by RBS modelling.

From the discussion above, it is evident that the strain state of *each* sample should be determined if a valid estimate of x is sought from XRD measurements. In principle, the layer composition can be determined from independent measurements of both of its lattice constants, c(InGaN) and a(InGaN), if we know Poisson's ratio for the layer. Uncertainty in the Poisson ratio will be less damaging to accuracy than uncertainties in the lattice constants. However, potentially large and uncontrollable uncertainties will arise if the layer is not uniform, for example if there is phase segregation, inhomogeneity of indium content (whether lateral or vertical) or inhomogeneous strain (such as a barrel distortion) in the epilayer.

We conclude that direct measures of alloy composition, by techniques that are insensitive to the structure, such as RBS, SIMS and EPMA, are preferable to those that *depend* on structural data, as does XRD. The chemical techniques are also capable of varying degrees of depth resolution. Similar and somewhat stronger objections apply to DALI (digitally aided lattice imaging) when used quantitatively in transmission electron microscopy. Nevertheless, both XRD and DALI are useful techniques when applied with care.

3. EXAFS of InGaN epilayers

A set of well characterized InGaN epilayers was examined with a view to assessing the use of EXAFS for quantitative determination of semiconductor alloy composition. At the same time, EXAFS' known sensitivity to local structure may be expected to yield unique information about sample nanostructure in favourable circumstances. The work described here extends and largely supersedes previous results.

EXAFS originates in the self-interference of the photoelectrons emitted by a target atom, as they scatter back from shells of neighbouring atoms. The chemical identity, radial distance and co-ordination number of the surrounding atom shells all play a part in determining the form of the resulting oscillations in the x-ray absorption spectrum. Usually, the EXAFS of a model environment is calculated and systematically refined, shell by shell, in order to match the experimental spectrum or its Fourier transform. In addition, the fitting procedure yields a measure of the combined structural and thermal disorder of the neighbouring atom shells through the familiar Debye–Waller (D–W) factors.

Samples of InGaN, approximately 2–300 nm thick, were grown on 2–3 micron thick GaN templates on sapphire, by metallorganic vapour phase epitaxy (MOVPE), as described in [9]. The structural, optical and compositional characteristics of these samples have also been investigated previously [10]. Our first objective is to test previous calibrations of the indium content, using the PL peak energy, measured conventionally, as a reference [5].

Indium K-edge EXAFS spectra of InGaN films were obtained at Station 9.2 of the UK Synchrotron Radiation Source at the Daresbury Laboratories. The storage ring operated at 2 GeV with currents between 250 and 120 mA. Spectra were recorded to 15 k (Å^{-1}) in fluorescence mode, with the samples at room temperature (296 K), using a Canberra solid state Ge detector with 13 elements. A Si (220) double-crystal monochromator was detuned to 70% of its maximum response in order to suppress harmonic contamination of the signal. The monochromator was calibrated using an indium foil, whose K edge was fixed at 27.926 eV. In some cases, scans were summed to obtain adequate data quality (see table 1). EXAFS of a high-quality sputtered layer of pure InN was also carried out as a calibration standard for both data acquisition and modelling [11].

The EXAFS data were reduced using the Daresbury computer programmes EXCALIB and EXBROOK and analysed in EXCURV98 [12]. The k^2-weighted data were simulated in k-space using phase shifts calculated *ab initio* from Von Barth ground state and Hedin–Lundqvist exchange potentials. The amplitude reduction factor was fixed at unity [13]. An introduction to EXAFS at Daresbury is provided in [14].

For each EXAFS simulation the validity of extra parameters was checked using a comparative reduced χ^2 method; the fit index R is also quoted as an absolute measure of the goodness of fit. The reduced χ^2 is defined by

$$\text{reduced } \chi^2 = \chi^2/(\mathrm{N}_i - \mathrm{N}_v)$$
$$\chi^2 = \sum_i^N \left(\frac{X_{data}(k_i) - X_{model}(k_i)}{\varepsilon_i} \right)^2 \tag{4}$$

where ε_i is the uncertainty at each point and X_{data} and X_{model} are the experimental and model values of the EXAFS at the point. N_i is the number of independent points defined as $[(2\,\Delta k\,\Delta r/\pi) + 1]$, where Δk is the range of data fitted in k-space, Δr is the range of data fitted in real space and N_v is the number of variables used in obtaining the fit.

In the reduced χ^2 test, the assumption is made that the uncertainty is the same at each point. Furthermore, the uncertainty in the theory is impossible to quantify accurately. Thus the values of reduced χ^2 given in the tables have been used for comparative purposes only.

Table 1. Local structure parameters of InGaN epilayers, determined by EXAFS, at 296 K.

Sample ID No of scans	Atom type	Number of atoms	Distance (Å)	Debye– Waller factor (Å^2)	Data range (Å^{-1}) R value Reduced χ^2
85	N	4	2.10(2)	0.011(1)	13
8	0.83(6) Ga/0.17 In	12	3.26(3)	0.012(1)	36.3
					6.4
336 (t)	N	4	2.10(2)	0.006(1)	10
4	0.77(6) Ga/0.23 In	12	3.28(3)	0.014(2)	48.4
	0.77(6) Ga/0.23 In	6	4.58(5)	0.006(1)	17.1
336 (m)	N	4	2.11(2)	0.007(2)	12
10	0.74(5) Ga/0.26 In	12	3.28(3)	0.013(2)	43.6
					13.0
336 (b)	N	4	2.11(2)	0.010(1)	12.5
10	0.67(5) Ga/0.33 In	12	3.29(3)	0.012(2)	57.9
					19.9
336 (d)	N	4	2.11(2)	0.006	13
4	0.62(4)Ga/0.38 In	12	3.29(3)	0.011(2)	45.5
					11.0

R is defined by the expression $R = \Sigma_i[(1/(\sigma_i))(|\text{experiment}(i) - \text{theory}(i)|] \times 100\%$, where

$$1/(\sigma_i) = [k(i)]^2/(\Sigma_i[k(i)]^2|\text{experiment}(i)|). \tag{5}$$

The initial model used to fit the InGaN data was a two-shell fit of four neighbouring N atoms and then 12 Ga atoms. This cluster was assigned a tetrahedral geometry and full cluster multiple scattering with up to three different scattering atoms in any scattering path with a maximum total path length of 12 Å. It was found that adding indium in a different shell did not give a better fit by the reduced χ^2 test to any of the spectra. However in most cases part-substituting indium into the gallium sites did give statistically better results and in one case (sample 336t) a second more distant metal shell is also seen in the EXAFS. Total co-ordination numbers were fixed during the refinement procedure as it was found that allowing these to vary did not improve the quality of the fit sufficiently, as measured by the reduced χ^2 test. Adding other shells of N or Ga also did not improve the simulation. The error in the In/Ga ratio in the second coordination sphere was estimated by studying the variation in the fit index in maps of the value of this ratio versus the Debye–Waller factor for this shell. Similar maps were used to estimate the error in the interatomic distances. The InGaN results are collected in table 1.

The InN data were fitted using full multiple scattering and a tetrahedral model, with four N atoms in the first shell, 12 In atoms in the second coordination sphere and a third shell of six In atoms. The addition of more N atoms to the model did not improve the value of the reduced χ^2 function. Results are listed in table 2.

Using lattice parameters of $a_{InN} = 3.536$ Å and $c_{InN} = 5.709$ Å yields the following interatomic separations (and occupation numbers) for the first few shells surrounding a central In atom in InN: N1, 2.153 Å (3), 2.169 Å (1); In1, 3.509 Å (6), 3.536 Å (6). The corresponding values from EXAFS modelling of the data (table 2) are N1, 2.16 Å (4); In1, 3.52 Å (12), which are seen to represent accurate averages over the respective subshells. The close agreement with the expected result acts as a consistency check for the analysis of the InGaN data that follows.

Figure 3 confirms the linear dependence of the peak energy of photoluminescence (PL) on the indium fraction, derived from the EXAFS fit for the first metal shell (table 1). Extrapolated

Table 2. Local structure of InN sputtered layer, determined by EXAFS.

Sample growth temperature No of scans	Atom type	Number of atoms	Distance (Å)	Debye–Waller factor (Å^2)	Data range (Å^{-1}) R value Reduced χ^2
500	N	4	2.16(2)	0.009(1)	14
2	In	12	3.53(3)	0.018(2)	26.6
	In	6	4.97(5)	0.024(3)	2.8

to zero x, the line of best fit meets the energy axis close to the band gap of pure GaN, as expected. The best-fit line (with error estimates in parentheses) is

$$E_p = 3.29(3) - 4.24(11)x \qquad \text{(EXAFS, five points)} \tag{6}$$

where E_p is the peak energy in eV and x is the indium fraction. This compares with an overall data fit

$$E_p = 3.41(3) - 4.36(16)x \qquad \text{(all data, 36 points)} \tag{7}$$

that was obtained by combining data from a number of studies, including this one, on the same sample set. (Sample inhomogeneity allows several data points to be obtained from each physical sample.) The other techniques comprised EPMA (17 datapoints) and RBS (14 datapoints). Inverting the relations provides a predictor of indium fraction from PL peak energy, with the EXAFS estimates consistently about 2% less than those obtained by using all the data.

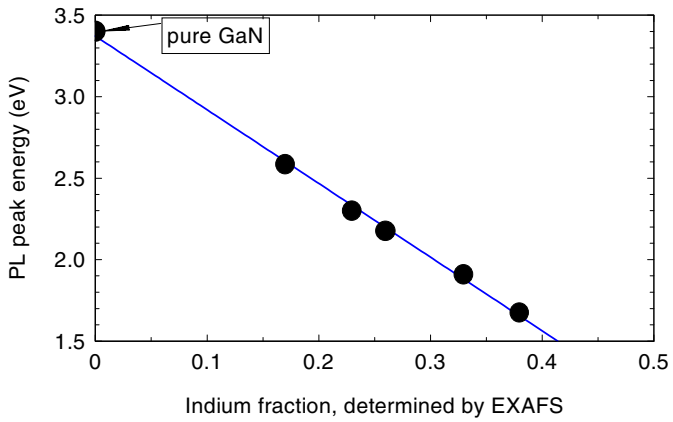

Figure 3. The dependence of PL peak energy on x, estimated from EXAFS modelling.

As described in section 2, Vegard's law allows an estimate of a relaxed alloy's composition from an x-ray measurement of its lattice constant (and *vice versa*) on the assumption that the lattice constant varies linearly with the composition. In figure 4 we compare, for all five samples, the shell radii, obtained from EXAFS modelling, with estimates of the same quantities derived using Vegard's law and the EXAFS-determined compositions. Using the more accurate compositions estimated from analysis of all the $E_p(x)$ data does not materially alter the following discussion.

For random alloys of InGaN that contain 17% to 38% indium nitride, the In–N1 radii predicted by Vegard's law, assuming a uniform expansion of the unit cell, span the range 1.98

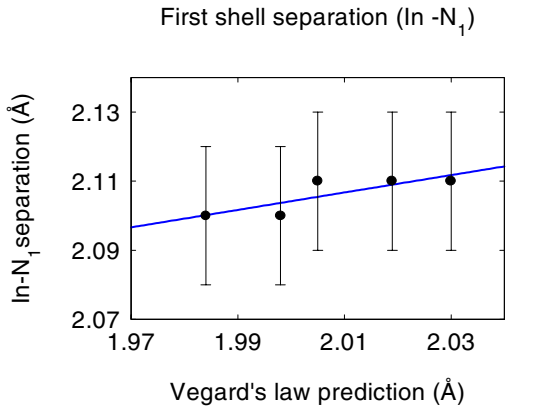

(a)

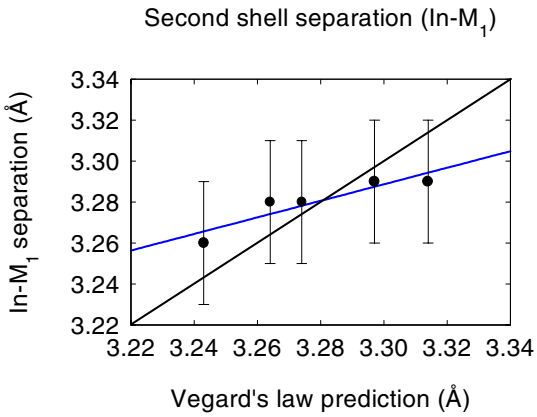

(b)

Figure 4. Local structure parameters of InGaN epilayers. See text for description.

to 2.03 Å. The radial distances determined in this EXAFS study are consistently higher. In fact, the In–N1 separation is found to be constant within the measurement error for all samples, with a mean value of 2.11(2) Å.

The thick line in figure 4(b) has been drawn to represent agreement between EXAFS and Vegard's law estimates of the In–M1 separation. This separation is geometrically equivalent to the in-plane lattice constant, a. The data deviate strongly from the Vegard's law prediction; the cation–cation nearest neighbour separation derived from EXAFS is approximately independent of composition. A statistical analysis shows that, given the uncertainty in the measurement of each data point, the slopes of the trendlines, drawn as thin lines through the data points in figure 4, do not differ significantly from zero. The mean radius of the first metal shell is 3.28(3) Å, very much closer to the GaN value (3.19 Å) than to that of InN (3.54 Å).

EXAFS-derived composition values are comparable with those estimated by use of established techniques. EXAFS also confirms the linear dependence of the PL peak energies on indium nitride fraction, over a wide range of composition. The approximately constant discrepancy of about 2% between EXAFS estimates and those of RBS and EPMA may be due to a systematic error, associated with the phase-shifts used in the data analysis. Because

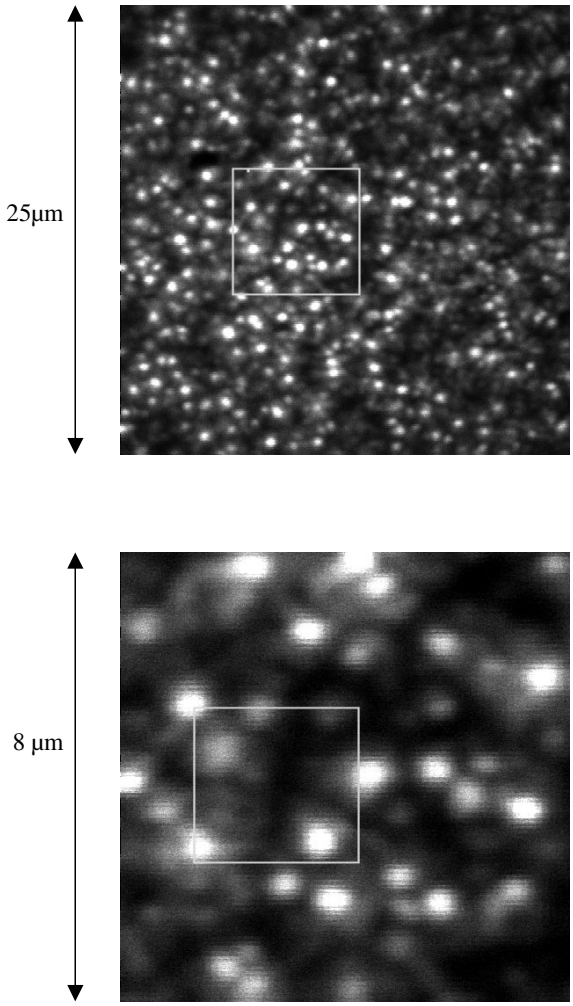

Figure 5. Spotty luminescence texture of InGaN, as revealed by confocal microscopy.

the phase shifts are calculated from theory, it is inappropriate to include a refinement of their values as another iterative step in the data fitting.

We conclude that EXAFS, using a simple model, provides a reasonably accurate means of determining semiconductor alloy composition. For InGaN alloys, the range of applicability of the technique extends from about 15% upwards, corresponding to light emission in the range from the blue to the infra-red. Samples with approximately 10% indium produced less reliable results than those described here, for two reasons [15]. Firstly, the sample absorption decreases with indium content, making the EXAFS signal more difficult to obtain in a reasonable time. Secondly, when the indium content is low, data fitting fails to discriminate sufficiently between increasingly similar situations, for example, scattering from a metal shell with 11 Ga atoms and one In atom, and from one containing gallium atoms only.

In addition to mean local composition, EXAFS provides structural information, in terms of interatomic spacings. For InGaN samples, these spacings appear to be very different from those expected from a consideration of Vegard's law. In particular, the structure appears to

vary little with composition and the nearest neighbour cation–anion separation, or bond length, 2.11(2) Å, seems to be anomalously large, closer to the value expected in pure InN (2.16 Å) than that found in GaN (1.95 Å). The influence of the effects of incomplete lattice relaxation in epilayers, discussed by Wu *et al* [16], (see also section 2), is not an issue here. Nor is there a possibility of systematic error, such as that discussed above in relation to InGaN composition estimates, since the structure obtained for the sample of pure InN is exactly what we expect from the accepted values of the lattice constants.

Matilla and Zunger, hereafter MZ, have performed a theoretical study of the local structure of InGaN alloys by valence force field simulations [17]. The level of detail available to such calculations has not been matched by our experimental models, but a few points of comparison may be noted. MZ calculate that the In–N1 bond length should be relatively insensitive to composition, as found experimentally, although the theoretical value is somewhat higher than the experimental. The calculated In–In1 and In–Ga1 separations are both substantially higher than the experimental values. We have not, however, been able to split the M1 shell in a consistent manner, in our EXAFS simulations. Also, the dependence of the theoretical In–M1 separations on composition follows Vegard's law predictions, while the experimental values do not. It is clearly important to compare the EXAFS structural determinations with the results of an XRD study of the same samples, in order to determine the strain state of these samples, assumed to be relaxed on account of their thickness. This matter is in hand.

The local environment of indium atoms in InGaN appears to be more like the distorted neighbourhood of size-mismatched impurity defects, substituting for host atoms, than that of an average site in a random alloy, even one decomposed into a number of sub-components. InN quantum dots, immersed in an InGaN matrix, probably occupy too small a total volume to be easily distinguished as a separate entity by EXAFS modelling. The fraction of indium atoms with complete shells of indium nearest neighbours is in any case likely to be rather small, since atoms near the surface of a dot will find themselves immediately adjacent to regions of crystal that are rich in gallium. No current model of the nanostructure of InGaN appears to be compatible with the EXAFS observation of a consistent local structure that is independent of the indium nitride fraction.

4. The nanostructure of InGaN light emitting layers

It is often said that the optical properties of InGaN depend upon its structure on the nanoscale. Here, we examine the reasons for supposing that this might be the case.

The high luminescence efficiency of InGaN materials and devices coexists with large densities of structural defects, identified by electron microscopy. If the structural defect densities are suppressed by sophisticated growth techniques, such as epitaxial lateral overgrowth, the luminescence efficiency does not markedly increase, although such growth procedures seem to be essential to ensure longevity in nitride laser devices [18]. The incorporation of indium nitride into gallium nitride in rather small amounts increases the luminescence efficiency by orders of magnitude, while shifting the PL emission peak energy only slightly [19]. When luminescent InGaN layers or devices are observed microscopically with sufficient resolution, the emitting surface takes on a granular or spotted appearance. An example of this distinctive luminescent texture is shown in figure 5. Bright spots stand out against a darker background (which is, however, also luminous). The lower limiting radius of the spots is comparable with the wavelength of light that they emit [20].

The above observations are consistent with the existence of distinct objects, containing indium, which have very high luminescence quantum efficiency. These objects compete very effectively with defects as centres for electron–hole recombination. Indeed, transmission

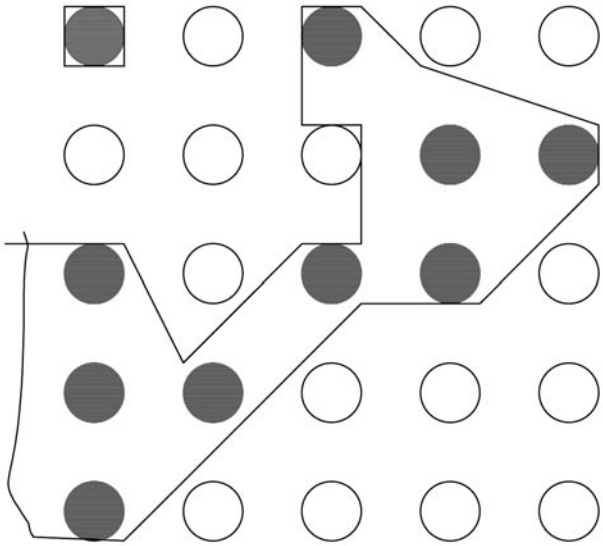

Figure 6. A sketch showing percolation clusters on a random two-component lattice, representing InGaN alloy.

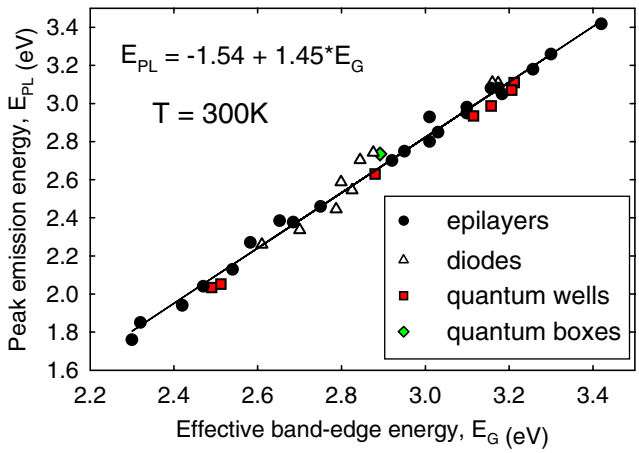

Figure 7. The correlation between the optical energies, E_g and E_{PL}, of representative InGaN samples.

electron micrographs of strongly luminescent material directly reveal objects that may be identified as quantum dots [21, 22]. Whether these objects are *responsible* for the luminescence is however an open question.

Some rather less direct evidence on the nature of these luminescent objects emerges from purely theoretical considerations. At most temperatures of growth, InGaN is not thermodynamically stable [23]. Like oil mixed with vinegar, InN, being insoluble in GaN, is supposed to form a suspension. The morphology of the dissolute InN is a matter for speculation.

Many authors have cited the possible role of alloy compositional fluctuations in localizing excitation. Presumably, however, this kind of localization occurs in all solid semiconductor

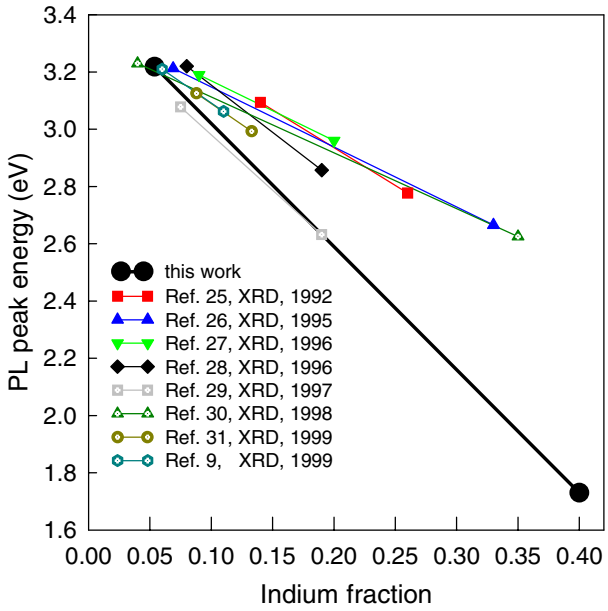

Figure 8. The dependence of the optical bandgap energy on indium nitride content in InGaN.

solutions, and cannot make InGaN stand out from the rest in the absence of some real structural oddities in the material. Finally, the present authors, and others, have speculated on the possibility of charge carriers or excitons becoming localized on percolation clusters of In atoms, such as those shown in figure 6, prior to electron–hole recombination [24]. The speculation that a common nanostructure, or a common localization mechanism, is responsible for InGaN luminescence, is reinforced by the observation of the universal optical behaviour exhibited by the materials.

The experimental and theoretical study of the dependence of the optical energies of InGaN on the InN fraction, x, has a chequered history. We conclude this review with a brief summary of recent progress. In discussing the InGaN literature, it is essential to compare like with like. Martin *et al* [6] introduced a description of the alloy bandgap, E_g, which can be measured in a consistent way by fitting the optical absorption or photoluminescence excitation spectra of epilayers, or the photovoltage spectra of diodes, to a sigmoidal function of energy. This procedure avoids the problem of equating the 'bandgap energy' with some arbitrary threshold in terms of the absorption strength.

There is less scope for confusion in comparing photoluminescence or electroluminescence spectra. These can be characterized, by the peak energies, pure and simple, of spectra taken under reproducible conditions. We denote these PL peaks by E_p.

When values of E_g and E_p are compared for a large number of samples, we find a strong correlation, as shown in figure 7. Remarkably, this figure includes data from thick and thin epilayers, from single and multiple quantum wells, from light emitting diodes, and from samples containing self-organized (SO) quantum boxes. The common thread that connects the optical properties of different InGaN structures seems to be the indium nitride content in the active layers. This is at least true for the thick epilayer samples, where we can easily measure the composition.

Turning briefly to this topic, we can say immediately that the linear dependence of the bandgap energy on the PL peak energy (figure 7) and that of the PL peak energy on the InN

fraction (figure 3) leads to a linear dependence of E_g on x. As explained previously, we can establish this relation only for thick epilayers, for which we can be confident of the value of x. The best numerical estimates at the time of writing are

$$E_g(x) = 3.44(12) - 3.0(3)x. \tag{8}$$

This relation is valid in the range $0 < x < 0.4$. Overestimation of the indium content by XRD (section 2) produced a consensus of anomalous results prior to about 1998/99, leading one eminent observer to remark that indium had been 'devalued' in that year! Some of these erroneous results are compared to equation (8) in figure 8.

Finally, the widely held belief that $E_g(x)$ *should be* quadratic in form has lead to further confusion, particularly among theorists, concerning the value of the 'bowing parameter'. There is no experimental evidence for such a bowing of the $E_g(x)$ relation, probably because no $In_xGa_{1-x}N$ samples with x in excess of 0.5 have been grown. Whatever the reason for the apparent linear dependences of the optical energies on the composition of InGaN, it is probably safe to say that a proper understanding of these dependences will be key to a future understanding of the influence of the structural on the optical properties of InGaN.

Acknowledgments

We would like to thank CLRC and EPSRC for the award of a number of Daresbury Direct Access grants for the EXAFS measurements, and S C Bayliss and co-workers of De Montfort University for early experimental assistance with these measurements. KPOD thanks Alex Zunger for helpful comments on the EXAFS data.

References

[1] Nakamura S and Fasol G 1997 *The Blue Laser Diode* (Berlin: Springer)
[2] Chichibu S, Azuhata T, Sota T and Nakamura S 1997 *Appl. Phys. Lett.* **70** 2822
[3] Chichibu S, Wada K and Nakamura S 1997 *Appl. Phys. Lett.* **71** 2346
O'Donnell K P, Martin R W and Middleton P G 1999 *Phys. Rev. Lett.* **82** 237
[4] Lester S D, Ponce F A, Craford M G and Steigerwald D A 1995 *Appl. Phys. Lett.* **66** 1249
[5] O'Donnell K P, Martin R W, White M E, Jacobs K, Van der Stricht W, Demeester P, Vantomme A, Wu M F and Mosselmans J F W 2000 *Mater. Res. Soc. Symp. Proc.* vol 595 (Pittsburgh, PA: Materials Research Society) p W11.26.1
[6] Martin R W, Middleton P G, O'Donnell K P and Van der Stricht W 1999 *Appl. Phys. Lett.* **74** 263
[7] O'Donnell K P, Martin R W, Trager-Cowen C, White M E, Esana K, Dealcher C, Middleton P G, Jacobs K, Van der Stricht W, Merlet C, Gil B, Vantonme A and Mosselmans J F W 2001 *Mater. Sci. Eng.* B **82** 194
[8] Wright A F 1997 *J. Appl. Phys.* **82** 2833
[9] Van der Stricht W 1999 *PhD Thesis* University of Ghent
[10] O'Donnell K P, Martin R W, Middleton P G, Bayliss S C, Fletcher I, Van der Stricht W, Demeester P and Moerman I 1999 *Mater. Sci. Eng.* B **59** 288
[11] Sample kindly provided by Guo Q; see O'Donnell K P, Martin R W, White M E, Mosselmans J F W and Guo Q 1999 *Phys. Status Solidi* b **216** 151
[12] Binsted N 1998 *EXCURV98* CCLRC Daresbury Laboratory Computer Program
[13] Roy M, Gurman S J and van Dorssen G 1997 *J. Physique Coll.* IV **7** C2 151
[14] Mosselmans J F W and Stephenson P 2000 http://srs.dl.ac.uk/xrs/index.html
[15] Mosselmans J F W 2000 unpublished results. See also [11]
[16] Wu M F, Vantomme A, Hogg S M, Langouche G, Van der Stricht W, Jacobs K and Moerman I 1999 *Appl. Phys. Lett.* **74** 365
[17] Mattila T and Zunger A 1999 *J. Appl. Phys.* **85** 160
[18] Nakamura S *et al* 1998 *Appl. Phys. Lett.* **72** 211
[19] Mukai T, Morita D and Nakamura S 1998 *J. Cryst. Growth* **189/190** 778
[20] O'Donnell K P, Martin R W, White M E, Tobin M J, Mosselmans J F W, Watson I M, Damilano B and Grandjean N 2000 *Proc. Mater. Res. Soc. (Boston, 2000)* at press

[21] Narukawa Y, Kawakami Y, Funato M, Fujita S, Fujita S and Nakamura S 1997 *Appl. Phys. Lett.* **70** 981
[22] Nistor L, Bender H, Vantomme A, Wu M F, Van Landuyt J, O'Donnell K P, Martin R W, Jacobs K and Moerman I 2000 *Appl. Phys. Lett.* **77** 507
[23] Ho I and Stringfellow G B 1996 *Appl. Phys. Lett.* **68** 2701
[24] O'Donnell K P 2001 *Phys. Status Solidi* a **183** 117
[25] Nakamura S and Mukai T 1992 *Japan. J. Appl. Phys.* **31** L1457
[26] Nakamura S 1995 *J. Vac. Sci. Technol.* A **13** 705
[27] Keller S, Keller B P, Kapolnek D, Abare A C, Masui H, Coldren L A, Mishra U K and DenBarrs S P 1996 *Appl. Phys. Lett.* **68** 3147
[28] Shan W, Little D B, Song J J, Feng Z E, Schurman M and Stall R A 1996 *Appl. Phys. Lett.* **69** 3315
[29] Takeuchi T, Takeuchi H, Sota S, Sakai H, Amano H and Akasaki I 1997 *Japan. J. Appl. Phys.* **36** L177
[30] Collection of early data from figure 16 of Bedair S M 1998 *Semicond. Semimet.* **50** 147
[31] Kwon Y-H, Gainer G H, Bidnyk S, Cho Y H, Song J J, Hansen M and DenBarrs S P 1999 *Appl. Phys. Lett.* **75** 2545